**PHOTONICS Research**

# Ultraflat, broadband, and highly coherent supercontinuum generation in all-solid microstructured optical fibers with all-normal dispersion

Chunlei Huang,[1,2] Meisong Liao,[1,*] Wanjun Bi,[1,2] Xia Li,[1] Lili Hu,[1] Long Zhang,[1] Longfei Wang,[1] Guanshi Qin,[3] Tianfeng Xue,[1,2] Danping Chen,[1] and Weiqing Gao[4] (iD)

[1]*Key Laboratory of Materials for High Power Laser, Shanghai Institute of Optics and Fine Mechanics, Chinese Academy of Sciences, Shanghai 201800, China*
[2]*University of Chinese Academy of Sciences, Beijing 100049, China*
[3]*State Key Laboratory on Integrated Optoelectronics, College of Electronic Science and Engineering, Jilin University, Changchun 130012, China*
[4]*School of Electronic Science & Applied Physics, Hefei University of Technology, Hefei 230009, China*
*Corresponding author: liaomeisong@siom.ac.cn*

High flatness, wide bandwidth, and high-coherence properties of supercontinuum (SC) generation in fibers are crucial in many applications. It is challenging to achieve SC spectra in a combination of the properties, since special dispersion profiles are required, especially when pump pulses with duration over 100 fs are employed. We propose an all-solid microstructured fiber composed only of hexagonal glass elements. The optimized fiber possesses an ultraflat all-normal dispersion profile, covering a wide wavelength interval of approximately 1.55 μm. An SC spectrum spanning from approximately 1030 to 2030 nm (corresponding to nearly one octave) with flatness <3 dB is numerically generated in the fiber with 200 fs pump pulses at 1.55 μm. The results indicate that the broadband ultraflat SC sources can be all-fiber and miniaturized due to commercially achievable 200-fs fiber lasers. Moreover, the SC pulses feature high coherence and a single pulse in the time domain, which can be compressed to 13.9-fs pulses with high quality even for simple linear chirp compensation. The Fourier-limited pulse duration of the spectrum is 3.19 fs, corresponding to only 0.62 optical cycles.    © 2018 Chinese Laser Press

## 1. INTRODUCTION

Comprising various dispersive and nonlinear effects, supercontinuum (SC) generation in fibers is a very active field of research that provides a high-brightness broadband optical source for a wide set of applications, such as optical coherence tomography, ultrashort pulse generation, and optical frequency metrology [1–3]. The high flatness, wide bandwidth, and high-coherence properties of SC are essential for some applications and are dominated by chromatic dispersion, pump pulse duration, and the spectral broadening mechanism [1,4]. Significant research efforts have been devoted to improving the properties [5–8].

Microstructured optical fibers (MOFs) offer remarkable design flexibility in modifying nonlinear coefficients and chromatic dispersion [9–11]. Numerous designs have involved the possibility of dispersion profiles with none or more than one

zero-dispersion wavelengths in MOFs [12–14]. Therefore, MOFs are particularly suitable for SC generation, and many impressive results have been achieved [15–17]. In general, SC generation in MOFs has been extensively explored using pump pulses in the anomalous dispersion regime [1,3,18]. The broadening mechanism is mainly dominated by soliton dynamics, dispersive waves, stimulated Raman scattering, and modulation instability. Soliton dynamics and dispersive wave effect can lead to fine structures in spectra, while stimulated Raman scattering and modulation instability can amplify the pulse noise [19–21]. Therefore, it is difficult to generate highly coherent and ultraflat SC spectra in the anomalous dispersion regime. In contrast, fibers without zero-dispersion wavelengths over the entire region of interest, known as all-normal dispersion (ANDi) fibers, are also currently employed as the nonlinear media [19,22]. SC generation in ANDi fibers is particularly appealing, as

the spectral broadening is mainly dependent on self-phase modulation (SPM) and optical wave-breaking (OWB). Both of the effects are self-seeded processes and can maintain smooth phase distribution as well as the integrity of the pump pulses in the time domain [23–25]. The intrinsic broadband noise owing to input shot noise and spontaneous Raman scattering can be successfully suppressed by using an ANDi fiber with maintaining polarization [26]. Therefore, SC generation in ANDi fibers feathers broadband flattop spectral profiles and high coherence.

Previous research has also demonstrated that SC generation in ANDi fibers can be characterized by flattop, broadband, and highly coherent properties. Heidt *et al.* demonstrated that coherent octave-spanning SC spectra with the flatness of better than 2 dB can be numerically achieved with a combination of a 50-fs pulse train at 1.08 μm with an air/silica glass fiber [19]. Another octave-spanning smooth SC spectrum (<3 dB) with 100-fs pulses at 1.55 μm was theoretically identified by Miret *et al.* [27]. The fiber, based on lead silicate glass, had many air holes with two different diameters; thus, it was difficult to precisely maintain the structures of the fiber during fabrication. Sukhoivanov *et al.* numerically investigated the optimization of dispersion profiles through multiorder dispersion engineering to generate broadband ultraflat SC spectra with 100-fs pulses at 1.55 μm [28]. Nevertheless, the dispersion profile of optical fibers designed was not well-matched for the target. Chatterjee *et al.* analyzed the effects of multiorder dispersions on the flatness of SC spectra and indicated that tailoring dispersion was important to generate ultraflat and broadband SC spectra [29]. Moreover, the octave-spanning SC with flatness <5 dB was theoretically achieved with a pulse width of 75 fs at 1.55 μm. Diouf *et al.* recently demonstrated a numerical work to generate a coherent mid-infrared SC covering from 2900 to 4575 nm at –3 dB in a chalcogenide fiber with 50-fs pulses [30]. Klimczak *et al.* reported an octave-spanning SC spectrum at –7 dB was generated in the honeycomb-lattice fiber pumped by 75-fs pulses at 1.55 μm [31,32]. Coherent SC spectra up to more than 2 μm have been achieved in an ANDi silica fiber with a germanium-doped core [33,34]. The pump pulse durations in the above research are not beyond 100 fs. It is worth noting that the bulky chirp compensation grating pair is essential in pump lasers with pulse durations below 100 fs [35]. In this case, the SC sources are clumpy and cannot be all-fiber systems, which are limited for many applications. However, the flatness of SC spectra degrades with an increase of pump pulse duration. A special ANDi could be an approach to achieve ultraflat SC generation with broader pump pulse duration, according to previous research [28,29].

In this paper, we propose an all-solid microstructured fiber with a hexagonal cladding composed only of high-index and low-index glass hexagons, which is impossible in air-glass MOFs. Based on a couple of silicate glasses, the optimized fiber exhibited ultraflat ANDi, covering a wide wavelength interval of approximately 1.55 μm. The experimental spectrum generated at 1.06 nm agreed well with that of the numerical simulation, despite the peak around the pump wavelength. A broadband SC spectrum with flatness <3 dB, spanning approximately 1030 to 2030 nm (corresponding to nearly one octave), is numerically generated in the fiber with 200-fs pump pulses at 1550 nm.

It is worth noting that –3 dB of spectral intensity corresponds to slightly higher than the half of the maximum spectral intensity; thus, the width at –3 dB of the maximum spectral intensity almost corresponds to the full width at half-maximum spectral intensity. The fiber lasers with 200-fs pulses are already commercially achievable; thus, the broadband ultraflat SC source can potentially be used in all-fiber systems. The SC spectrum possesses high coherence and preserves a single pulse in the temporal domain, which was well suited for pulse recompression. The SC spectrum allows the compression to 13.9-fs pulses (2.69 optical cycles) with high quality by only linear chirp compensation. The Fourier-limited pulse duration of the spectrum is 3.19 fs, corresponding to only 0.62 optical cycles.

## 2. FIBER DESIGN AND CHARACTERISTICS

Before the fabrication of the all-solid MOF, it is necessary to carefully select thermally and mechanically compatible glasses to avoid cracking at the core-cladding interface. In our experiment, we considered the development of the all-solid MOF with pairs of silicate glasses, labeled as G1 ($62.5SiO_2$-$13.3CaO$-$6.4Na_2O$-$6.4BaO$-$2.3TiO_2$-$4.4K_2O$-$4ZnO$-$0.7Al_2O_3$, mol. %) and G2 ($82.1SiO_2$-$7.5K_2O$-$9.8Na_2O$-$0.6BaO$, mol. %), respectively. The glasses exhibit outstanding properties of resistance to recrystallization in thermal processing. It is striking that the glasses selected have similar thermophysical properties, thus being thermally and chemically compatible, as shown in Table 1. In the Table, $n_d$ denotes the refractive index at 587.6 nm; $T_g$ and $T_s$ are the transformation temperature and the softening point of glass, respectively, and $\alpha$ is the linear thermal expansion coefficient for the temperature range 100°C–300°C. From these properties, we can see that G1 and G2 glasses have good compatibility and are appropriate in drawing fiber. Therefore, cracking at the core-cladding interface can be avoided.

The transverse cross section of the typical MOF proposed in this paper is schematically shown in Fig. 1(a), where low-index regions are shown in white, high-index regions are shown in dark gray, and they alternate. The structure is composed of hexagonal elements, shown by the blue lines in Fig. 1(a). The microstructured cladding is hexagonal and composed of periodic structures, including one high-index ring and one low-index ring, denoted as pitch $\Lambda$. The core is formed by one high-index region, including a few rings considered as a defect, which is characterized by the number of rings $n$. Therefore, the fiber is characterized by three parameters: the pitch $\Lambda$, the number of rings included in the core $n$, and the number of periodic structures in the microstructured cladding $N$. Figure 1(b) shows the refractive index profiles along with the $x$ axis of the fiber cross section. The guidance mechanism is the total internal reflection effect. In the fiber, G1 glass with higher refractive index was considered as the core, and the high-index

**Table 1.    Some Critical Parameters of G1 and G2**

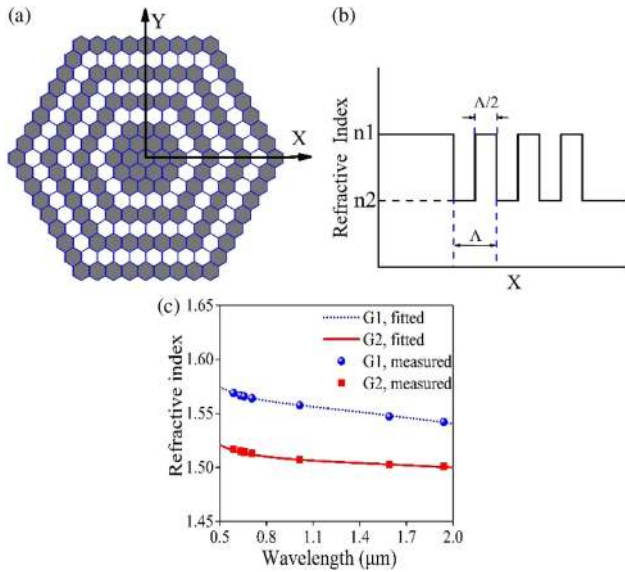| Glass | $n_d$ | $T_g$ (°C) | $T_s$ (°C) | $\alpha$ ($10^{-7}$/K) |
|-------|-------|-----------|-----------|----------------------|
| G1 | 1.56883 | 581 | 642 | 90 |
| G2 | 1.51680 | 560 | 620 | 95 |

**Fig. 1.** (a) Schematic cross section and (b) refractive index profile of the all-solid microstructured fiber. The blue lines show the hexagonal elements. (c) Refractive index curves of G1 and G2 glasses.
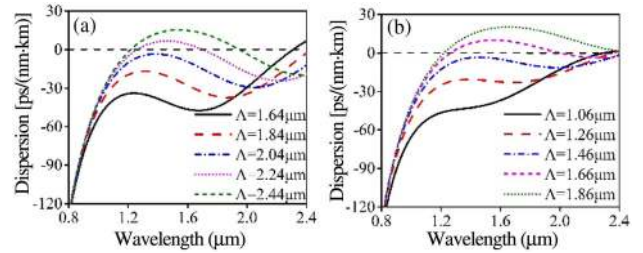


**Fig. 2.** Calculated spectral dependence of chromatic dispersion for all-solid MOF structures with various parameters of (a) $\Lambda = 1.64$–$2.44$ μm, $n = 3$ and (b) $\Lambda = 1.06$–$1.86$ μm, $n = 4$.

hexagonal rods in cladding structures. G2 glass was used for the background.

In order to analyze optical properties of the fiber related to geometrical parameters, the numerical model of the fiber was built. The modes were calculated using a finite-difference eigenmode solver. Field distribution, chromatic dispersion, and confinement loss of the modes were calculated using the full-vectorial finite-difference method based on perfectly matched layer boundary conditions. As shown in Fig. 1(c), the measured refractive indices of both glasses were fitted to the Sellmeier formula [36]:

$$n^2(\lambda) - 1 = \sum_{i=1}^{3} \frac{B_i \lambda^2}{\lambda^2 - C_i}. \tag{1}$$

Here, $n(\lambda)$ is the refractive index, $\lambda$ is the wavelength in micrometers. $B_i$ and $C_i$ are the Sellmeier coefficients, which are tabulated in Table 2.

Figure 2 shows the numerical dispersion profiles for various values of pitch $\Lambda$, while three periodic structures were employed. Three rings are included in the core in Fig. 2(a), and four are included in Fig. 2(b); thus, $n = 3$ and $n = 4$, respectively. It can be readily observed that the increase in pitch $\Lambda$ results in uplifting of the chromatic dispersion profiles, and the saddles in the profiles become flatter and broader. In Fig. 2(a), the dispersion of the fiber in the structure with $\Lambda < 2.24$ μm is all-normal and the local maximum dispersion wavelengths are redshifted as the pitch $\Lambda$ increases. The dispersion

becomes anomalous for the structure with $\Lambda = 2.24$ μm at the wavelength near 1.5 μm, which was not expected. As shown in Fig. 2(b), the chromatic dispersion profiles of the fiber with $n = 4$ also upshift with an increase of the pitch. Note that the fiber with $n = 4$ presents flatter dispersion profiles than the fiber with $n = 3$. In the structure with $\Lambda = 1.46$ μm, the dispersion ranges from −3.3 to −13 ps/(nm·km), covering from 1.2 μm to above 2.35 μm.

Although the fiber has flat dispersion, only three factors of tailoring dispersion limit design flexibility, which does not allow fine engineering of the dispersion and generating ultraflat SC spectra. In order to enhance the design freedom of the fiber to a large extent, we considered breaking the periodicity of the cladding rings, since every ring in the structure profoundly influences the dispersion. Figures 3(a) and 3(b) show two typical structures in which two and four diagonal low-index hexagons in the first inner ring are replaced by high-index hexagons, labeled as fiber #A and fiber #B, respectively. The pitch is 1.84 μm and $n = 3$. The dispersion profiles of fiber #A and fiber #B are presented in Fig. 3(c). For comparison, the dispersion of the fiber with a normal periodic structure is also shown, and other parameters were considered the same. Compared to the normal fiber, dispersion of fiber #A and fiber #B appears flatter.

By trial and error, we selected one structure, shown in Fig. 4(a), labeled as fiber #C. In this structure, all low-index hexagons at the vertices in the first inner ring are replaced by
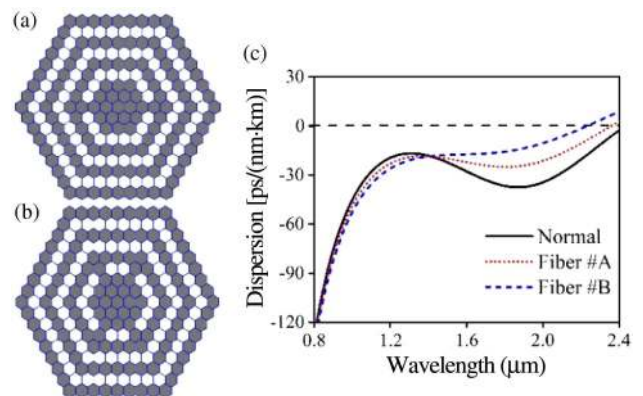
**Table 2. Sellmeier Coefficients of G1 and G2**

| Glass | $B_1$ | $B_2$ | $B_3$ | $C_1$ | $C_2$ | $C_3$ |
|-------|-------|-------|-------|-------|-------|-------|
| G1 | 1.172 | 0.2552 | 1.6380 | 0.005661 | 0.02447 | 117.2 |
| G2 | 1.045 | 0.2196 | 0.7548 | 0.005207 | 0.02722 | 176.5 |



**Fig. 3.** Schematic cross section of (a) fiber #A and (b) fiber #B; (c) calculated spectral dependence of chromatic dispersion of fiber #A and fiber #B.
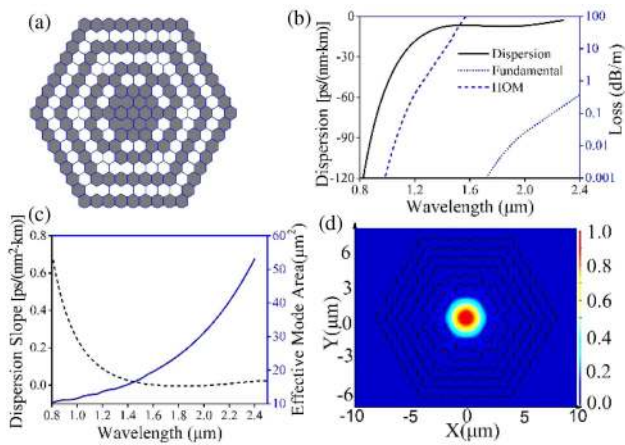
**Fig. 4.** (a) Schematic cross section of fiber #C; (b) calculated chromatic dispersion and confinement losses of fundamental mode and the first HOM; (c) calculated values of dispersion slope and effective mode area of fundamental mode; (d) electric field distribution of the fundamental mode at 1550 nm.

high-index hexagons, and all high-index hexagons at the vertices in the second inner ring are replaced by low-index hexagons. The pitch is 1.91 μm. The chromatic dispersion of the fiber is presented in Fig. 4(b). The local maximum dispersion at a wavelength of 1.65 μm is –6.7 ps/(nm · km). The dispersion profile remains ultraflat, with dispersion values between –5 and –9 ps/(nm · km) from 1.45 to 2.14 μm. The dispersion slope is shown in Fig. 4(c). In the fiber, we achieved a low dispersion slope, between –0.02 and 0.1 ps/(nm² · km) from 1.2 to 2.4 μm. The confinement losses of the fundamental mode and the first higher-order mode (HOM) with respect to wavelength are shown in Fig. 4(b). The confinement loss of the fundamental mode is below 1 dB/m over 0.8–2.4 μm, while the loss of the first HOM is beyond 10 dB/m at 1.5 μm. Therefore, the fiber can be considered as a single-mode fiber over 1.5 μm. The effective mode area with respect to wavelength is presented in Fig. 4(c), and the electric field distribution of the fundamental mode is also presented in Fig. 4(d). The effective nonlinear coefficients of the fiber at 1.06 and 1.55 μm are approximately 19 and 9.5 $W^{-1} \cdot km^{-1}$ for nonlinear refractive index $n_2 = 3.9 \times 10^{-20}$ m²/W according to the Boling–Glass–Owyoung model [37,38]:

$$n_2(10^{-13} \text{ m}^2/\text{W})$$
$$= \frac{68 (n_d - 1)(n_d^2 + 2)^2}{2.387 \times 10^6 \, n_0 \, v_d \left[1.517 + \frac{(n_d^2+2)(n_d-1)\times v_d}{6n_d}\right]^{0.5}}. \quad (2)$$

Here, $v_d$ is the Abbe number, and $n_d$ is the refractive index at 587.6 nm.

## 3. FIBER FABRICATION

The fiber #C was fabricated. During fiber drawing, we employed the stack-and-draw method because the method is common, low-cost, and easy to operate. First, we put a high-index rod of 20-mm diameter into a furnace and draw into rods
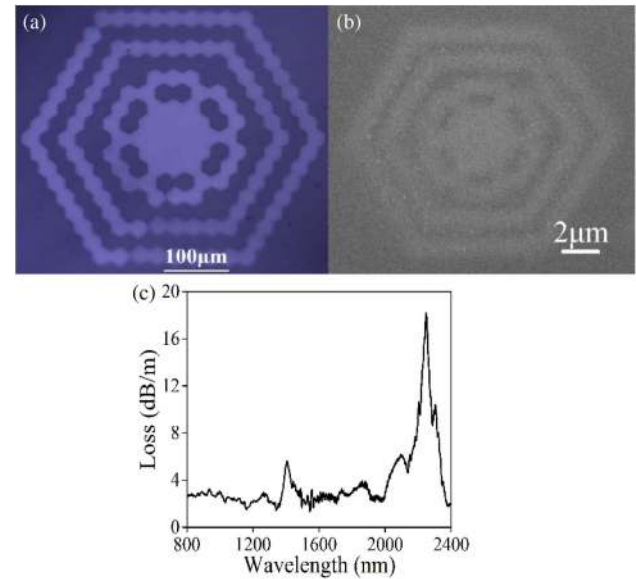


**Fig. 5.** Pictures of cross sections of (a) the fabricated cane under an optical microscope and (b) the fiber under scanning electron microscope; (c) measured propagation loss of the fiber.

with 1-mm diameter, and we did the same for a low-index rod. Then, we used the small rods to stack the objective structure and draw the cane with 1-mm diameter. The cross section of the cane is shown in Fig. 5(a). Note that all the glass rods become hexagonal. In the stacked structure, there was a small space among three adjacent circular rods, and the spaces were equally filled by the rods during the heating process. In addition, the cladding structure in the cane distorted slightly, but the distortion only has a very minute influence on the dispersion, which is negligible. Next, the cane was stacked with low-index glass rods, which is a preform. Finally, the preform was placed in a furnace and drawn into fiber. The cross section of the fiber is shown in Fig. 5(b). The structure was well maintained, and the diameter of the fiber is 300 μm. The propagation loss of the fiber was measured by the method of cutting back, as shown in Fig. 5(c). The measured loss was at the level of 1.5–4 dB/m at wavelengths covering from 0.8 to 2.4 μm, while the strong loss peaks at 1.38 and 2.2 μm are 5.6 and 18.2 dB/m attributed to hydroxyl group OH absorption, respectively [34]. The relative strength at 1.38 and 2.2 μm is approximately identical to that given by Humbach *et al.* [39]. Although the preform was isolated from atmospheric water during fiber drawing in the nitrogen gas atmosphere, the hydroxyl group OH in the fiber cannot be completely removed due to the limited conditions in our laboratory. The propagation loss was expected to decrease down to a low level by removing the hydroxyl group OH and optimizing the fabrication procedure.

## 4. SC GENERATION

The ANDi fiber #C was considered to generate a broadband ultraflat SC spectrum. The evolution of the ultrashort pulse propagating along the fiber in the time domain can be described by the generalized nonlinear Schrödinger equation [36]:

$$\frac{\partial A}{\partial z} = -\frac{\alpha}{2}A + \sum_{k \geq 2}\frac{i^{k+1}}{k!}\beta_k\frac{\partial^k A}{\partial T^k} + i\gamma\left(1 + i\tau_{shock}\frac{\partial}{\partial T}\right)$$

$$\times \left[A(z, T)\int_{-\infty}^{\infty} R(T_1)|A(z, T - T_1)|^2 dT_1\right], \quad \textbf{(3)}$$

where $A$ is the pulse envelope, $z$ is the distance of propagation, $\beta_k$ is the dispersion coefficients, $T$ is the co-moving frame at the envelope group velocity, $\alpha$ is the linear loss, and $\gamma$ is nonlinear coefficient. In this paper, the constant nonlinear coefficient at the pump wavelength was used [22]. Shock term $\tau_{shock} = 1/\omega_0$ is also included. $R(t)$ is the Raman response function,

$$R(t) = (1 - f_R)\delta(t) + f_R\frac{\tau_1^2 + \tau_2^2}{\tau_1\tau_2^2}\exp\left(-\frac{t}{\tau_2}\right)\sin\left(\frac{t}{\tau_1}\right).$$

$$\textbf{(4)}$$

We employed the Raman response parameters from Schott glass SF57, namely $t_1 = 5.5$ fs, $t_2 = 32$ fs [40]. The fractional contribution of the delayed Raman to nonlinear polarization is 0.1.

### A. SC Generation at 1060 nm

In order to verify the calculated dispersion, we carried out an experiment on SC generation at 1.06 μm and made comparisons with the numerically simulated results. Excitation pulses with a pulse width of 50 fs for the fiber are provided by a laser with an average power of 2.2 W and a repetition rate of 70 MHz. The laser was coupled into the fiber with an aspheric lens. The output SC light was launched into a large-mode-area optical fiber connected with an optical spectrum analyzer (Yokogawa, AQ6370C). The output power was measured by a power meter. The coupling efficiency was ~10%.

Figure 6 shows the experimentally recorded SC spectrum generation in a 20-cm long piece of the fiber, plotted on a logarithmic scale. The fiber length supported the spectral broadening sufficiently, as well as avoided the fiber loss having an influence on the SC spectrum. Note that there was a strong peak around the pump wavelength in the recorded spectrum, which was assigned to the partial pump energy propagation in the cladding. We also plotted the spectrum of the pump pulse propagation in the cladding of the fiber. The profile and
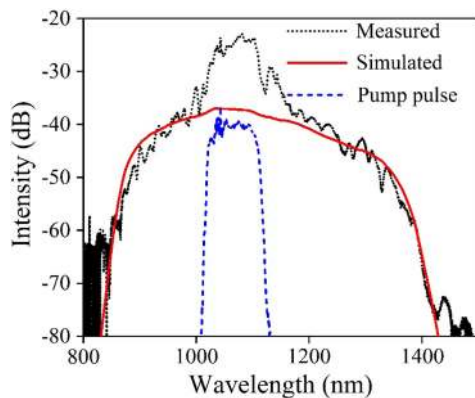
**Fig. 6.** Experimentally recorded and simulated SC spectra after 20 cm of the optical fiber. The pump pulse duration was 50 fs at 1.06 μm in both cases.

location of the spectrum of the pump pulses were in agreement with those of the peak. The SC spectrum covered from 830 to 1460 nm and agreed well with that of the numerical simulation, despite the peak around the pump wavelength. The small discrepancies between the profiles arise from the fact that the pump pulses are slightly different from the simulation.

### B. SC Generation at 1550 nm

Previous research has shown that pumping near the local maximum dispersion was required to achieve optimal spectral width and flatness [19,22]. Having no access to an ultrashort pulse laser of 1.55 μm in our laboratory, we numerically investigated the SC generation in the fiber. In our simulations, we considered hyperbolic-secant input pulses at a wavelength of 1.55 μm with a pulse duration of 200 fs and peak power of 100 kW. The parameters of the pump pulses are already achievable in commercial erbium-doped fiber lasers. The propagation length was kept at 1 m. The nonlinear loss is not included.

Figures 7(a) and 7(b) show the spectral evolution process with propagation distance on a logarithmic scale in the fiber. In the initial propagation of the ultrashort pulse in the optical fiber, spectral broadening exhibits deep oscillations, and the achievable bandwidth is narrow, mainly dominated by SPM, as shown in Fig. 7(c). With further propagation, as shown in Fig. 7(a), two sidelobes occurred on both sides of the spectrum, which is due to the OWB effect. New frequencies are dramatically generated via a degenerate four-wave mixing effect related to OWB on the trailing pulse edge and the leading pulse edge in the time domain. It is worth noting that spectral broadening occurred earlier in the high-frequency regime. The
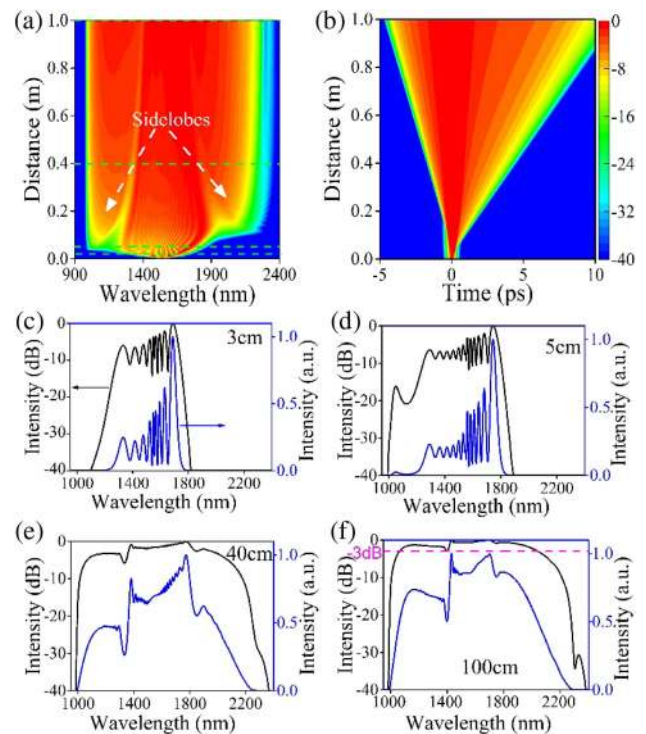
**Fig. 7.** (a) Spectral and (b) temporal evolution dependence on propagation distance; spectrum profiles at propagation distances of (c) 3 cm, (d) 5 cm, (e) 40 cm, and (f) 1 m. The green dashed lines in panel (a) chronologically show the location of panel.

self-steepening effect is responsible for the earlier onset of OWB in the short wavelength region [19,41]. During these processes, the spectral bandwidth is fundamentally saturated, but the energy around pump wavelength is transferred to the new frequency band. At the onset of OWB, the spectrum is not symmetric and flat, as shown in Fig. 7(d). With further propagation along the fiber, the energy is further transferred by nonlinear and dispersive effects, and the spectra are smoother, as shown in Figs. 7(e) and 7(f). It is worth noting that the energy is slowly accumulated in the short wavelength regime during pulse propagation. For instance, the spectrum in Fig. 7(f) is much flatter than that in Fig. 7(e); thus, the pulse propagation distance affects spectral flatness. We can imagine that the flatness will become worse when pulses further propagate over a certain distance. In other words, there is a propagation interval that supports the best flatness.

In Fig. 7(f), in a logarithmic scale, the spectrum profile exhibits a smooth flattop and steep edges and is almost rectangular. The SC spectrum shows high flatness with deviations of less than 3 dB covering from approximately 1030 to 2030 nm, corresponding to nearly an octave. Compared with results of previous papers [19,27–29], the pump pulse duration is much longer. As shown in the above section, the dispersion possesses high flatness near the local maximum dispersion, and the local maximum dispersion is slightly normal to balance nonlinearity and dispersion effects. Therefore, the dispersion allows longer pump pulse duration to generate the SC spectrum with the flatness <3 dB according to Heidt *et al.* [42]. Because hyperbolic-secant input pulses with a pulse duration of 200 fs and peak power of 100 kW at 1.55 μm are achievable from the commercially erbium-doped fiber lasers, the broadband ultraflat SC sources may feather all-fiber properties. It is worth noting that −3 dB of spectral intensity corresponds to slightly higher than the half of the maximum spectral intensity; thus, the width at −3 dB of the maximum spectral intensity almost corresponds to the full width at half-maximum spectral intensity.

Going one step further, we compared the generated spectra for different pulse durations after 1-m propagation in fiber #C. The pulse durations were set as 100, 200, and 300 fs. In all cases, the peak power is 100 kW. The numerical results on a logarithmic scale are shown in Fig. 8. It is clear that the flatness of the spectrum with 300 fs duration is the poorest, while the flatness with 100-fs pulses is better than the others. Note that
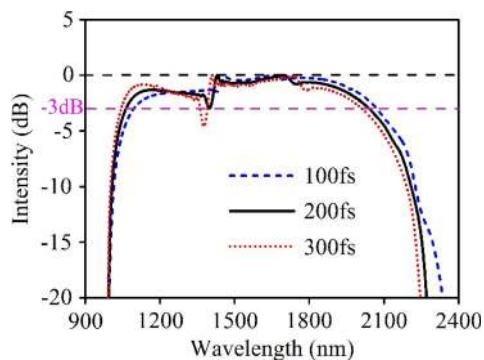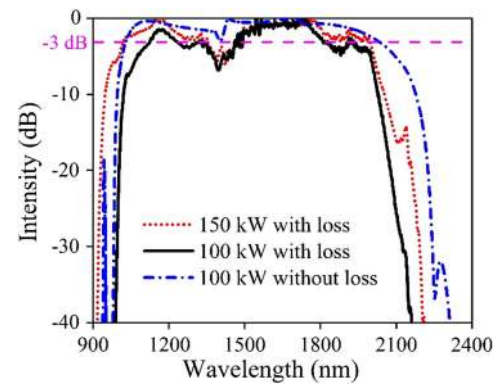


**Fig. 9.** Influence of linear loss on SC generation after a fiber of 1 m in length. The pump pulse durations are 200 fs at 1.55 μm. The peak power is 100 kW and 150 kW, respectively.

the dip in the short wavelength interval near the pump pulses is the main factor reducing the flatness. Increasing the pump pulse duration results in deeper dip; thus, it is more difficult to generate ultraflat SC spectra in ANDi fibers pumped with broad duration pulses. In order to obtain ultraflat SC spectra, it is crucial to tailor dispersion profiles to reduce the dip depth of SC spectra.

We also analyzed the influence of the loss on the spectral flatness, and the results are shown in Fig. 9. The spectrum generated in a fiber with loss is narrower and has much finer structures compared to the spectrum without loss. For a given fiber, the generated spectral bandwidth is dependent on the peak power of pump pulses. During broadening, the pulse intensity is weakened due to the propagation loss, which dampens the wavelength components generated. In addition, the strong loss at 1.38 μm seriously affects the flatness of the SC spectrum. The fine structures can be explained by the fact that the fiber is long enough, and large fluctuation in the fiber loss becomes significant. In order to obtain broadband SC with high flatness, we performed numerical simulations of SC generation using the peak power of 150 kW. The result is shown in Fig. 9. Without considering the region at 1.38 μm, the spectral bandwidth at −3 dB covers from 1030 to 2000 nm, which is approximately identical to that of the SC generated in the fiber without the loss with the peak power of 100 kW. The result indicates that the influence of the loss on the bandwidth and flatness of the SC spectrum can be to some extent weakened by increasing the peak power of the pump pulses, while the strong loss at 1.38 μm still seriously degrades the spectral flatness, and the loss at 2.2 μm prevents spectral broadening for the long wavelength regime. Therefore, for obtaining high spectral flatness, the hydroxyl group OH should be removed, and the fiber loss should have small fluctuation.

## 5. COHERENCE AND PULSE COMPRESSION

We also analyzed the coherence of the SC spectrum generated in the fiber without the linear loss. The modulus of the complex degree of coherence was used [43]. Input pulse shot noise is semiclassically modeled by using one photon per mode, and 100 simulations in each series were performed. In this paper, $t_1 - t_2 = 0$ is used.



**Fig. 8.** SC spectrum profiles after 1 m of propagation with pumping durations of 100 fs (blue dashed line), 200 fs (black solid line), and 300 fs (red dotted line). The peak power is 100 kW at 1.55 μm.
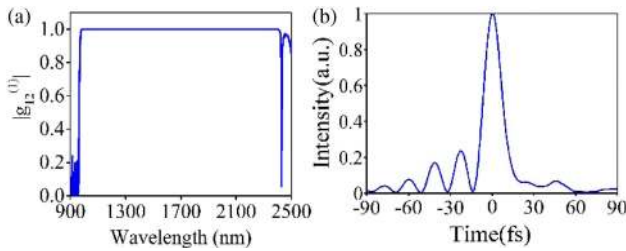
**Fig. 10.**   (a) Computed modulus of the complex degree of coherence of SC spectrum; (b) achievable pulse width only using linear compression.

Figure 10(a) shows the modulus of the complex degree of coherence after 1-m propagation distance in fiber #C. It is clear that the modulus is equal to one covering the wavelength range from 950 to approximately 2400 nm, corresponding to high coherence. The high coherence is determined by SPM and OWB. During the SPM process, the intensity-dependent phase shift generated new frequencies, and then the mixing of overlapping frequency components coming from SPM generated other new frequencies in the OWB process. In both dynamics, noise cannot be amplified, and the pulses maintain integrality. Therefore, the SC spectra can maintain the coherence property of the pump laser. Note that, as shown in Fig. 7(b), the pulse can still preserve a single-pulse structure, which is crucial for pulse compression.

Based on the above analysis, the spectrum with 200-fs pump pulses possesses high coherence and maintains integrality of pulses, which determines the high compressibility of SC pulses. Therefore, simulation of pulse compression was carried out. In this simulation, we only considered second-order dispersion compensation, which can be satisfied using a simple grating or a prism pair [20,44,45]. The result is shown in Fig. 10(b), where the pulses are compressed using a piece of fiber of 1 m in length. The full width at half-maximum of the pulse is 13.9 fs, corresponding to 2.69 optical cycles at a central wavelength of 1550 nm, and the pulse exhibits a relatively good quality. Owing to the propagation length, both sides of the main pulse are contained in a broad pedestal, since the wavelength components experience a high amount of nonlinear chirp. Using more sophisticated compression methods, such as a $4f$ pulse shaper, the pulse may be compressed to its bandwidth-limited pulse duration of 3.19 fs, corresponding to only 0.62 optical cycles [46]. This result shows that the SC generation in the ANDi fiber not only has high coherence and maintains a single pulse in the time domain but exhibits broadband and ultraflat spectral properties.

## 6. CONCLUSION

We proposed an all-solid MOF with a hexagonal cladding composed only of hexagonal high-index and low-index glass hexagons, which is impossible in MOFs with air holes. Such a hexagonal structure appears to be attractive, as it offers simplicity as well as great freedom in design flexibility to engineer dispersion, which can easily be fabricated by a standard stack-and-draw technique. Based on a couple of silicate glasses, the optimized fiber exhibits ultraflat ANDi, covering a wide

wavelength interval of approximately 1.55 μm. The experimental spectrum generated at 1.06 nm agreed well with that of the numerical simulation. A broadband SC spectrum with flatness <3 dB, spanning from approximately 1030 to 2030 nm (corresponding to nearly one octave), is numerically generated in the fiber with 200-fs pump pulses at 1550 nm. It is worth noting that –3 dB of spectral intensity corresponds to slightly higher than the half of the maximum spectral intensity; thus, the width at –3 dB of the maximum spectral intensity almost corresponds to the full width at half-maximum spectral intensity. The results indicate that the broadband ultraflat SC sources can be all-fiber and miniaturized due to commercially achievable 200-fs fiber lasers.

We also analyzed the influence of the loss on the spectral flatness. The propagation loss dampens wavelength components generated and seriously affects spectral flatness. Although the influence of the loss on the bandwidth and flatness can be to some extent weakened by increasing the peak power of the pump pulses, the strong loss at 1.38 μm still seriously degrades the spectral flatness, and the loss at 2.2 μm prevents spectral broadening for the long wavelength regime. Therefore, for obtaining high spectral flatness, the hydroxyl group OH should be removed, and the fiber loss should have small fluctuation.

The ultraflat SC generation exhibits a high degree of coherence and a single pulse in the time domain, allowing the compression to 13.9-fs high-quality pulses considering only linear chirp compensation. The Fourier-limited pulse duration of the spectrum is 3.19 fs, corresponding to only 0.62 optical cycles. The outstanding pulse compression capability in ultrashort pulse generation is ascribed to great flatness and high coherence of the broadband SC spectrum.

In addition, we also demonstrated that pump pulses with durations beyond 100 fs result in deep dips; thus, it is difficult for ultraflat SC spectra to be generated in ANDi fibers pumped with broad duration pulses. To achieve ultraflat SC spectra, it is crucial to tailor dispersion profiles to reduce the dip depth of SC spectra.

## REFERENCES

1. J. M. Dudley, G. Genty, and S. Coen, "Supercontinuum generation in photonic crystal fiber," Rev. Mod. Phys. **78**, 1135–1184 (2006).
2. M. Tsuzuki, L. Jin, M. Yamanaka, V. Sonnenchein, H. Tomita, A. Sato, T. Ohara, Y. Sakakibara, E. Omoda, H. Kataura, T. Iguchi, and N. Nishizawa, "Midinfrared optical frequency comb based on difference frequency generation using high repetition rate Er-doped fiber laser with single wall carbon nanotube film," Photon. Res. **4**, 313–317 (2016).
3. M. Klimczak, B. Siwicki, A. Heidt, and R. Buczynski, "Coherent supercontinuum generation in soft glass photonic crystal fibers," Photon. Res. **5**, 710–727 (2017).
4. A. M. Heidt, J. S. Feehan, J. H. V. Price, and T. Feurer, "Limits of coherent supercontinuum generation in normal dispersion fibers," J. Opt. Soc. Am. B **34**, 764–775 (2017).
5. X. Liu, J. Laegsgaard, R. Iegorov, A. S. Svane, F. O. Ilday, H. Tu, S. A. Boppart, and D. Turchinovich, "Nonlinearity-tailored fiber laser

technology for low-noise, ultra-wideband tunable femtosecond light generation," Photon. Res. **5**, 750–761 (2017).

6. Z. Zheng, D. Ouyang, J. Zhao, M. Liu, S. Ruan, P. Yan, and J. Wang, "Scaling all-fiber mid-infrared supercontinuum up to 10 W-level based on thermal-spliced silica fiber and zblan fiber," Photon. Res. **4**, 135–139 (2016).

7. S. Vyas, T. Tanabe, M. Tiwari, and G. Singh, "Chalcogenide photonic crystal fiber for ultraflat mid-infrared supercontinuum generation," Chin. Opt. Lett. **14**, 123201 (2016).

8. B. B. Yan, J. H. Yuan, X. X. Sang, K. R. Wang, and C. X. Yu, "Combined nonlinear effects for UV to visible wavelength generation in a photonic crystal fiber," Chin. Opt. Lett. **14**, 050603 (2016).

9. J. C. Knight, "Photonic crystal fibres," Nature **424**, 847–851 (2003).

10. P. St. J. Russell, "Photonic crystal fibers," Science **299**, 358–362 (2003).

11. J. C. Knight, T. A. Birks, P. St. J. Russell, and D. M. Atkin, "All-silica single-mode optical fiber with photonic crystal cladding," Opt. Lett. **21**, 1547–1549 (1996).

12. M. Chemnitz, J. Wei, C. Jain, B. P. Rodrigues, T. Wieduwilt, J. Kobelke, L. Wondraczek, and M. A. Schmidt, "Octave-spanning supercontinuum generation in hybrid silver metaphosphate/silica step-index fibers," Opt. Lett. **41**, 3519–3522 (2016).

13. M. Liu, B. Zhao, X. Yang, and J. Hou, "Seven-core photonic liquid crystal fibers for simultaneous mode shaping and temperature sensing," Chin. Opt. Lett. **15**, 060601 (2017).

14. P. S. Maji and R. Das, "Designing broadband fiber optic parametric amplifier based on near-zero single ZDW PCF with ultra-flat nature," Chin. Opt. Lett. **15**, 070606 (2017).

15. N. Nishizawa and J. Takayanagi, "Octave spanning high-quality supercontinuum generation in all-fiber system," J. Opt. Soc. Am. B **24**, 1786–1792 (2007).

16. C. Strutynski, P. Froidevaux, F. Desevedavy, J. C. Jules, G. Gadret, A. Bendahmane, K. Tarnowski, B. Kibler, and F. Smektala, "Tailoring supercontinuum generation beyond 2 μm in step-index tellurite fibers," Opt. Lett. **42**, 247–250 (2017).

17. Z. K. Dong, Y. R. Song, R. Q. Xu, Y. Zheng, J. R. Tian, and K. X. Li, "Broadband spectrum generation with compact Yb-doped fiber laser by intra-cavity cascaded Raman scattering," Chin. Opt. Lett. **15**, 071408 (2017).

18. A. V. Husakou and J. Herrmann, "Supercontinuum generation of higher-order solitons by fission in photonic crystal fibers," Phys. Rev. Lett. **87**, 203901 (2001).

19. A. M. Heidt, "Pulse preserving flat-top supercontinuum generation in all-normal dispersion photonic crystal fibers," J. Opt. Soc. Am. B **27**, 550–559 (2010).

20. S. Demmler, J. Rothhardt, A. M. Heidt, A. Hartung, E. G. Rohwer, H. Bartelt, J. Limpert, and A. Tunnermann, "Generation of high quality, 1.3 cycle pulses by active phase control of an octave spanning supercontinuum," Opt. Express **19**, 20151–20158 (2011).

21. A. Hartung, A. M. Heidt, and H. Bartelt, "Design of all-normal dispersion microstructured optical fibers for pulse-preserving supercontinuum generation," Opt. Express **19**, 7742–7749 (2011).

22. A. M. Heidt, A. Hartung, G. W. Bosman, P. Krok, E. G. Rohwer, H. Schwoerer, and H. Bartelt, "Coherent octave spanning near-infrared and visible supercontinuum generation in all-normal dispersion photonic crystal fibers," Opt. Express **19**, 3775–3787 (2011).

23. L. Liu, T. L. Cheng, K. Nagasaka, H. T. Tong, G. S. Qin, T. Suzuki, and Y. Ohishi, "Coherent mid-infrared supercontinuum generation in all-solid chalcogenide microstructured fibers with all-normal dispersion," Opt. Lett. **41**, 392–395 (2016).

24. A. M. Heidt, J. Rothhardt, A. Hartung, H. Bartelt, E. G. Rohwer, J. Limpert, and A. Tunnermann, "High quality sub-two cycle pulses from compression of supercontinuum generated in all-normal dispersion photonic crystal fiber," Opt. Express **19**, 13873–13879 (2011).

25. C. L. Huang, M. S. Liao, W. J. Bi, X. Li, L. F. Wang, T. F. Xue, L. Zhang, D. P. Chen, L. L. Hu, Y. Z. Fang, and W. Q. Gao, "Asterisk-shaped microstructured fiber for an octave coherent supercontinuum in a sub-picosecond region," Opt. Lett. **43**, 486–489 (2018).

26. Y. Liu, Y. B. Zhao, J. Lyngso, S. X. You, W. L. Wilson, H. H. Tu, and S. A. Boppart, "Suppressing short-term polarization noise and related

spectral decoherence in all-normal dispersion fiber supercontinuum generation," J. Lightwave Technol. **33**, 1814–1820 (2015).

27. J. J. Miret, E. Silvestre, and P. Andres, "Octave-spanning ultraflat supercontinuum with soft-glass photonic crystal fibers," Opt. Express **17**, 9197–9203 (2009).

28. I. A. Sukhoivanov, S. O. Iakushev, O. V. Shulika, E. Silvestre, and M. V. Andres, "Design of all-normal dispersion microstructured optical fiber on silica platform for generation of pulse-preserving supercontinuum under excitation at 1550 nm," J. Lightwave Technol. **35**, 3772–3779 (2017).

29. S. K. Chatterjee, S. N. Khan, and P. R. Chaudhuri, "Designing a two-octave spanning flat-top supercontinuum source by control of nonlinear dynamics through multi-order dispersion engineering in binary multi-clad microstructured fiber," J. Opt. Soc. Am. B **32**, 1499–1509 (2015).

30. M. Diouf, A. Ben Salem, R. Cherif, H. Saghaei, and A. Wague, "Super-flat coherent supercontinuum source in $As_{38.8}Se_{61.2}$ chalcogenide photonic crystal fiber with all-normal dispersion engineering at a very low input energy," Appl. Opt. **56**, 163–169 (2017).

31. T. Martynkien, D. Pysz, R. Stepien, and R. Buczynski, "All-solid microstructured fiber with flat normal chromatic dispersion," Opt. Lett. **39**, 2342–2345 (2014).

32. M. Klimczak, B. Siwicki, P. Skibinski, D. Pysz, R. Stepien, A. Heidt, C. Radzewicz, and R. Buczynski, "Coherent supercontinuum generation up to 2.3 μm in all-solid soft-glass photonic crystal fibers with flat all-normal dispersion," Opt. Express **22**, 18824–18832 (2014).

33. K. Tarnowski, T. Martynkien, P. Mergo, K. Poturaj, A. Anuszkiewicz, P. Bejot, F. Billard, O. Faucher, B. Kibler, and W. Urbanczyk, "Polarized all-normal dispersion supercontinuum reaching 2.5 μm generated in a birefringent microstructured silica fiber," Opt. Express **25**, 27452–27463 (2017).

34. K. Tarnowski, T. Martynkien, P. Mergo, K. Poturaj, G. Sobon, and W. Urbanczyk, "Coherent supercontinuum generation up to 2.2 μm in an all-normal dispersion microstructured silica fiber," Opt. Express **24**, 30523–30536 (2016).

35. F. Li, Q. Li, J. H. Yuan, and P. K. A. Wai, "Highly coherent supercontinuum generation with picosecond pulses by using self-similar compression," Opt. Express **22**, 27339–27354 (2014).

36. G. P. Agrawal, *Nonlinear Fiber Optics* (Academic, 2007).

37. N. L. Boling, A. J. Glass, and A. Owyoung, "Empirical relationships for predicting non-linear refractive-index changes in optical solids," IEEE J. Quantum Electron. **14**, 601–608 (1978).

38. M. Feng, A. K. Mairaj, D. W. Hewak, and T. M. Monro, "Nonsilica glasses for holey fibers," J. Lightwave Technol. **23**, 2046–2054 (2005).

39. O. Humbach, H. Fabian, U. Grzesik, U. Haken, and W. Heitmann, "Analysis of OH absorption bands in synthetic silica," J. Non-Cryst. Solids **203**, 19–26 (1996).

40. V. L. Kalashnikov, E. Sorokin, and I. T. Sorokina, "Raman effects in the infrared supercontinuum generation in soft-glass PCFs," Appl. Phys. B **87**, 37–44 (2007).

41. C. Finot, B. Kibler, L. Provost, and S. Wabnitz, "Beneficial impact of wave-breaking for coherent continuum formation in normally dispersive nonlinear fibers," J. Opt. Soc. Am. B **25**, 1938–1948 (2008).

42. A. M. Heidt, A. Hartung, and H. Bartelt, "Generation of ultrashort and coherent supercontinuum light pulses in all-normal dispersion fibers," in *The Supercontinuum Laser Source*, R. R. Alfano, ed. (Springer, 2016), pp. 247–280.

43. M. H. Frosz, "Validation of input-noise model for simulations of supercontinuum generation and rogue waves," Opt. Express **18**, 14778–14787 (2010).

44. F. Krausz and M. Ivanov, "Attosecond physics," Rev. Mod. Phys. **81**, 163–234 (2009).

45. M. Miranda, T. Fordell, C. Arnold, A. L'Huillier, and H. Crespo, "Simultaneous compression and characterization of ultrashort laser pulses using chirped mirrors and glass wedges," Opt. Express **20**, 688–697 (2012).

46. Y. Liu, H. Tu, and S. A. Boppart, "Wave-breaking-extended fiber supercontinuum generation for high compression ratio transform-limited pulse compression," Opt. Lett. **37**, 2172–2174 (2012).